Morphological change from nano-cube to nano-sphere by addition of Ni to W in RF thermal plasma synthesis

Young-Min Kim[*], Hyunwoong Na[*], Wonsik Lee[*],
Byeong-Joo Lee[**], Nong-Moon Hwang[***], Hanshin Choi[*]

[*]Korea institute of industrial technology, 406-840 Incheon, Republic of Korea, ymkim77@kitech.re.kr, nhw@kitech.re.kr, wonslee@kitech.re.kr, hschoi@kitech.re.kr
[**]POSTECH, 790-784 Pohang, Republic of Korea, calphad@postech.ac.kr
[***]Seoul National University, 151-742 Seoul, Republic of Korea, nmhwang@snu.ac.kr

ABSTRACT

Tungsten and tungsten/nickel nano-particles were synthesized by feeding thermo-physically favorable feedstock micro-powders into argon-hydrogen thermal plasma. Tungsten nano-particle from tungsten trioxide micro-powder consisted of α-W nano-cube and β-W nano-sphere. Meanwhile, W/Ni nano-particle was composed of mainly α-W and β-W phases but nano-cube could not be identified. The morphological change from pure tungsten nano-cube to W/Ni nano-sphere was considered from atomistic simulation and it is concluded that the surface enriched nickel caused facet-defacet surface transition.

Keywords: tungsten nano-particle, tungsten/nickel nano-particle, radio frequency thermal plasma, Monte Carlo simulation

1 INTRODUCTION

Nano-particle synthesis and application technology have been intensively explored with advancements of fundamental studies and mass production processes [1]. Metallic nano-particles especially have superior electrical and thermal conductivity, so they can be used for electrical /thermal management of electronic components besides the conventional applications for catalyst [2-3]. Most of metallic nano-particles used in industries are composed of pure metals. However, it is necessary to develop metallic nano-particles composed of two or more components for various industrial applications. When it comes to metallic nano-particle synthesis method, solid base processes, liquid base processes, and vapor base processes are possible [4-6]. Each process has its own advantages and disadvantages. In the present study, RF thermal plasma process with solid powder feedstock is evaluated. RF thermal plasma synthesis of nano-particle belongs to vapor phase condensation technology in which nano-particle nucleates from supersaturated vapor and it grows by either heterogeneous condensation or collision /coalescence [7]. In regard to nano-particle synthesis by RF thermal plasma, it provides us with wide material selectivity and process facility owing to high energy density and reactivity of thermal plasma. During the process, feedstock micro-powders are fed into thermal plasma and they individually interact with thermal plasma. At the heating stage, solid powder is finally vaporized and then vapor is cooled by introduction of quench gas. With respect to process ability, vaporization degree of feedstock is a critical step for nano-particle synthesis: productivity of nano-particle is primarily dependent on vaporization rate [8]. Though thermal plasma has a high energy density, it is difficult to vaporize refractory metal. Therefore, thermo-physically favorable feedstock selection is important. In the case of bimetallic nano-particle synthesis, process reliability for chemical composition is another challenge in RF thermal plasma synthesis.

In the present study, W and W-Ni nano-particles were tried to be synthesized by RF thermal plasma process. When characteristics of tungsten nano-particle are compared to those of W/Ni nano-particle, nano-cube in tungsten nano-particle disappears with addition of nickel. It is considered from facet-defacet surface morphology change by atomistic simulation.

2 EXPERIMENTAL PROCEDURE

2.1 Nano-particle synthesis

W and W/Ni nano-particles were synthesized by reactive RF thermal plasma process. For pure W nano-particle, WO_3 micro-powder was fed into argon-hydrogen thermal plasma while a blended feedstock of WO_3 and $Ni(OH)_2$ micro-powder was used for W/Ni bimetallic nano-particle. Weight fraction of $Ni(OH)_2$ in blended feedstock was 0.25. Process parameters are summarized in Table 1. Hydrogen gas, as a reducing agent, is introduced through the sheath gas and its flow rate is sustained far above stoichiometric quantity for full reduction of oxide feedstock materials. Characteristics of as-synthesized nano-particles were conducted by x-ray diffractometry, transmission electron microscopy, and energy dispersion spectroscopy.

Table 1 Reactive RF thermal plasma process parameters

Feedstock				Plasma gas				
Feedstock	Feed-rate	Plasma power	Pressure	Central gas	Carrier gas	Sheath gas	Sheath gas	Quench gas
WO_3(100g) / WO_3(75g) – $Ni(OH)_2$(25g)	5gmin^{-1}	28kw	14.7psia	Ar 5slpm	Ar 5slpm	Ar 60slpm	H_2 5slpm	N_2 5slpm

2.2 Atomistic Simulation

The equilibrium shape evolution of pure W and W-Ni alloy nanoparticles has been investigated by a Monte Carlo atomistic simulation study based on Modified Embedded Atom Method (MEAM) [9, 10] interatomic potential for pure W [11], pure Ni [12] and W-Ni alloy systems [13]. To do this, two initially spherical nanoparticles of the same diameter of 6 nm (with 7144 atoms) were prepared and then morphological evolutions were seen at 1,200°C.

3 RESULTS AND DISCUSSION

Morphology and phase of both WO_3 feedstock micro-powder and as-synthesized W nano-particle are shown in Fig. 1. Blocky WO_3 micro-powder has a mean particle size of 25 um. As for the as-synthesized W nano-particle, nano-particle is synthesized as shown in Fig. 1 (b) after RF thermal plasma and mean particle size was 20 nm. It is noted that nano-cube and nano-sphere are present together and it is further confirmed from the STEM image of Fig. 1 (c). In addition, tungsten nano-particles consist of bcc α-W and β-W without any oxide phases as shown in Fig. 1 (d). β-W is of A 15 structure which is stabilized by interstitial impurity. In the W-O binary system, it is regarded as W_3O phase but it has a relatively large oxygen content range. Presence of β-W in the present study is likely to be due to incomplete reduction of vaporized tungsten species in spite of high energy density and active hydrogen atom of thermal plasma. Through the result, it is proven that morphological change from micro-powder to nano-particle by vaporization and condensation phase transformation and phase evolution from oxide feedstock to metallic particle via hydrogen reduction reaction are effectively achieved through the Ar-H_2 thermal plasma.

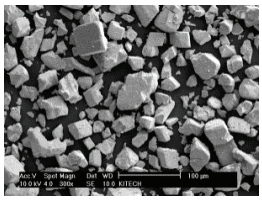

(a) WO_3 feedstock micro-powder

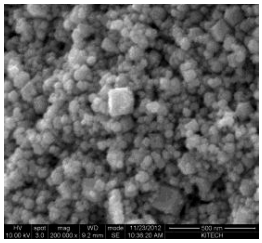

(b) FE-SEM image of as-synthesized particle

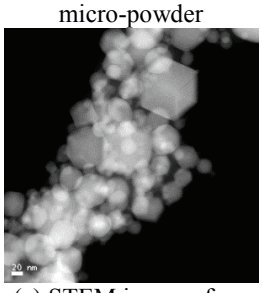

(c) STEM image of as-synthesized particle

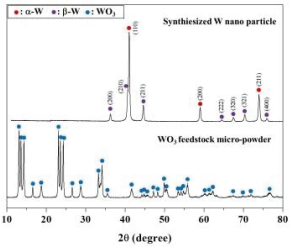

(d) X-ray diffraction patterns

Figure 1 Characteristics of tungsten trioxide feedstock powder and as-synthesized W nano-particle

In order to verify correlation between morphology (nano-cube and nano-sphere) and phase (α-W and β-W) of the as-synthesized W nano-particle, TEM analysis was intensively conducted. Figure 2 reveals that nano-cube is α-W phase and lattice spacing measured from square surface corresponds to (110) plane.

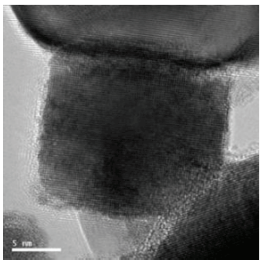

(a) Morphology of nano-cube

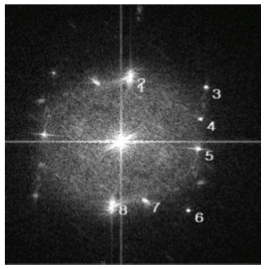

(b) FFT diffraction pattern of (a)

Figure 2 Identification of tungsten nano-cube

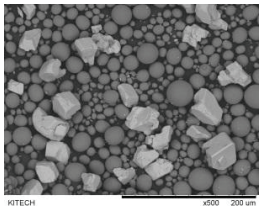

(a) WO_3-$Ni(OH)_2$ blended feedstock

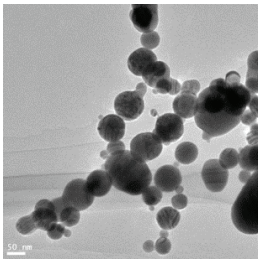

(b) As-synthesized W/Ni nano-particle

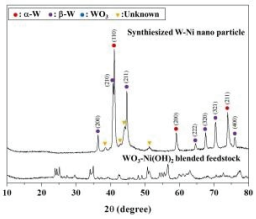

(c) X-ray diffraction patterns

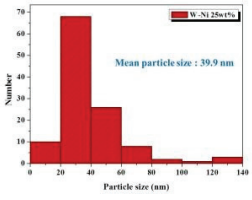

(d) Size distribution of W/Ni nano-particle

Figure 3 Characteristics of WO_3 and $Ni(OH)_2$ blended feedstock and as-synthesized W/Ni nano-particle

When it comes to W/Ni binary system, vaporization and reduction of oxide micro-powders are pre-requisite step and W/Ni nano-particle is nucleated from vapor containing tungsten and nickel species by following heterogeneous condensation. Comparison of morphology and phase composition between blended feedstock and as-synthesized particle reveal that reactive RF thermal plasma is valid for bimetallic nano-particle synthesis from blended oxide micro-powder, as shown in Fig. 3. With respect to phase composition of W/Ni nano-particle, both α-W and β-W are clearly identified and fcc γ-Ni cannot be indexed. The other peaks in the XRD pattern are well consistent with NiW phase but it needs further investigation because of the debates on the presence of NiW. Considering phase equilibrium of W-Ni

binary system, W has a negligible solubility of Ni while Ni has a significant solubility of W. Accordingly, it can be deduced that tungsten and nickel are condensed simultaneously because of steep temperature gradient during cooling and however, nickel is expelled outward without stabilizing fcc structure owing to lower nickel content in condensed particle.

When it comes to the chemical composition, it was measured by areal quantification of EDS analysis at the low magnification of x500 of SEM for 5 times and mean value was calculated. Weight fraction of W/(W+Ni) in blended feedstock is 0.79 and the measured W weight fraction of W/Ni nano-particle is 0.80. Exact coincidence between target chemistry and as-synthesized particle is an indirect evidence for full vaporization of blended feedstock during the process. Meanwhile, chemical composition was measured at the particle level using STEM-EDS in which probe diameter is less than 1 nm. Chemical composition at the particle level shows a significant distribution from 4 wt. % to 64 wt. % of nickel as shown in Fig. 4 (a). It is worthwhile to note that all the particles contain nickel on them and minimum measured tungsten content is 35.7 which is far higher than solubility limit of fcc Ni (approximately 31 wt.% in W-Ni binary phase diagram). Figure 4 (b) shows nano-particle morphology and its chemical composition. Though α-W is present, nano-cube is not clearly identified for the W/Ni nano-particle within the wide range of nickel content.

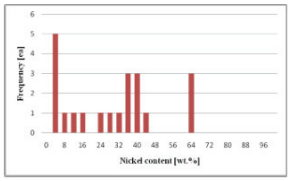

(a) Chemical composition

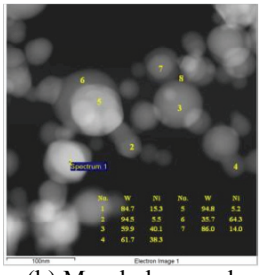

(b) Morphology and chemical composition

Figure 4 STEM-EDS analysis for as-synthesized W/Ni nano-particles

Morphological change from nano-cube of pure α-W to nano-sphere with Ni addition is considered by atomistic simulation from the viewpoint of the facet-defacet transition of metal surface. The shapes of the pure W and the W-Ni alloy particles after 5000 Monte Carlo steps (MCS: steps per atom) at 1200 ^{o}C are shown in Figs. 5 (a) and 5 (b), respectively. The two samples are seen from the same crystallographic orientation. It is clearly shown that the pure W particle is well faceted while the W-Ni alloy particle is rather spherical with surface enrichment of nickel element. The well-developed facet on the surface of pure W indicates the strong surface energy anisotropy characteristic of a singular interface. According to the present MEAM parameters, the computed surface energies of the (100), (110) and (111) surfaces of pure W are 3900, 3427 and 4341 erg/cm^2, respectively [11]. Among the three low-index surfaces (110) has the lowest surface energy and (111) has the highest. However, in case of pure Ni, the corresponding values are 1943, 2057 and 1606 erg/cm^2 for (100), (110) and (111) surfaces, respectively [12]. The (111) surface has the lowest energy while (110) has the highest, which is the opposite to the case of pure W. Therefore, the segregated Ni-rich layer on the surface seems to disturb the order of surface energies among surfaces of pure W, that is, the anisotropy of surface energy of pure W is lost due to the alloyed Ni. In other words, the alloyed Ni decreases the edge energy. A spherical particle with defaceted surfaces as shown in Fig. 5(b) can be obtained when the surface energy is rather isotropic or when the edge energy is small or close to zero. The surface segregation of alloyed Ni and its disturbance of surface energy anisotropy seem to cause the facet-defacet surface transition of W powders. Even though a large amount of Ni (14 at. %) was added in the present simulation, the necessary amount of alloying elements that can cause the surface transition would be much smaller in a real experimental situation as is deduced from result of Fig. 4 because the real powder size is much larger and the surface-to-volume ratio should be much smaller than that of the present samples.

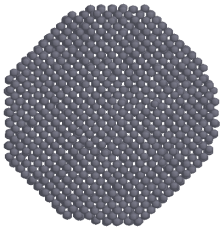

(a) Pure W particle

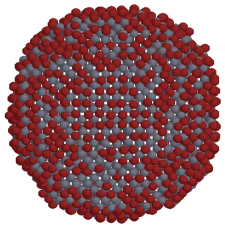

(b) W-Ni alloy particle (14 at. %)

Figure 5 Change of shape and atomic configurations of powders after the present Monte Carlo simulation at 1200^{o}C. The light gray (gray) and dark gray (red) spheres represent W and Ni atoms, respectively.

4 CONCLUSION

W and W/Ni nano-particles were synthesized by reactive RF thermal plasma using thermo-physically favorable WO_3 and $Ni(OH)_2$ micro-powder. Through the morphological change and phase evolution, it is proven that vaporization, reduction of in-flight oxide particle and condensation from vaporized species are effectively embodied. Nominal chemical composition is exactly consistent with target chemistry for W/Ni nano-particle. In the case of tungsten nano-particle, α-W nano-cube and β-W nano-sphere are identified. Meanwhile, nano-cube is not observed for W/Ni nano-particle though both tungsten phases are identified in XRD analysis. Through the atomistic simulation, it is concluded that α-W and β-W are present in both W and W/Ni nano-particles and presence of nickel affects morphological change from nano-cube to nano-sphere of α-W within the scope of this study.

ACKNOWLEDGEMENT

The authors appreciate the financial support from "ISTK Convergence Research Project" of MKE (Ministry of Knowledge Economy) and ISTK (Korea Research Council for Industrial Science and Technology) of Republic of Korea.

REFERENCES

[1] Daniel L. Fdldheim, Colby A. Jr. Foss, (2002) "Metal Nanoparticles: Synthesis, Characterization, and Applications," Marcel Dekker, New York, 2002

[2] G. Y. Huang, S. M. Xu, G. Xu, L. Y. Li, L. F. Zhang, "Preparation of fine nickel powders via reduction of nickel hydrazine complex precursors," Trans. Nonferrous Met. Soc. China 19, pp.389−393, 2009.

[3] H. Kishi, Y. Mizuno, H. Chazono, "Base-metal electrode multilayer ceramic capacitors: Past, present, and future perspectives," J. Appl. Phys. 42, pp.1−15, 2003.

[4] K. H. Kim, Y. B. Lee, E. Y. Choi, H. C. Park, S. S. P, "Synthesis of nickel powders from various aqueous media through chemical reduction method," Materials Chemistry and Physics 86, pp.420-424, 2004.

[5] S. Stopić, J. Nedeljković, Z. Rakočević, D. Uskoković, "Influence of Additives on the properties of spherical nickel particles prepared by ultrasonic spray pyrolysis," J. Mater. Res. 14(7), pp.3059-3065, 1999.

[6] R. Y. Chen, K. G. Zhou, "Preparation of ultrafine nickel powder by wet chemical process," Trans. Nonferrous Met. Soc. China 16, pp.1223-1227, 2006

[7] S. Son, M. Taheri, E. Carpenter, V.G. Harris, M. E. McHenry, "Synthesis of ferrite and nickel ferritte nano particles using radio-frequency thermal plasma torch," J. Appl Phys. 91, pp.7589-7591, 2002.

[8] H. Zhang, L. Bai, P. Hu, F. Yuan, J. Li, "Single-step pathway for the synthesis of tungsten nanosized powders by RF induction thermal plasma," Int. Journal of Refractory Metals and Hard Materials 31, pp.33–38, 2012.

[9] M.I. Baskes, "Modified embedded-atom potentials for cubic materials and impurities," Phys. Rev. B **46**, pp.2727-2742, 1992.

[10] B.-J. Lee and M.I. Baskes, "Second nearest-neighbor modified embedded-atom-method potential," Phys. Rev. B. **62**, pp.8564-8567, 2000.

[11] B.-J. Lee, M.I. Baskes, H. Kim and Y.K. Cho, "Second nearest-neighbor modified embedded atom method potentials for bcc transition metals," Phys. Rev. B. **64**, 184102 pp.1-11, 2001.

[12] B.-J. Lee, J.-H. Shim and M.I. Baskes, "Semiempirical atomic potentials for the fcc metals Cu, Ag, Au, Ni, Pd, Pt, Al, and Pb based on first and second nearest-neighbor modified embedded atom method," Phys. Rev. B. **68**, 144112 pp.1-11, 2003.

[13] J.-H. Shim, S.I. Park, Y.W. Cho and B.-J. Lee, "Modified embedded-atom method calculation for the Ni–W system," J. Mater. Res. 18, pp.1863-1867, 2003.